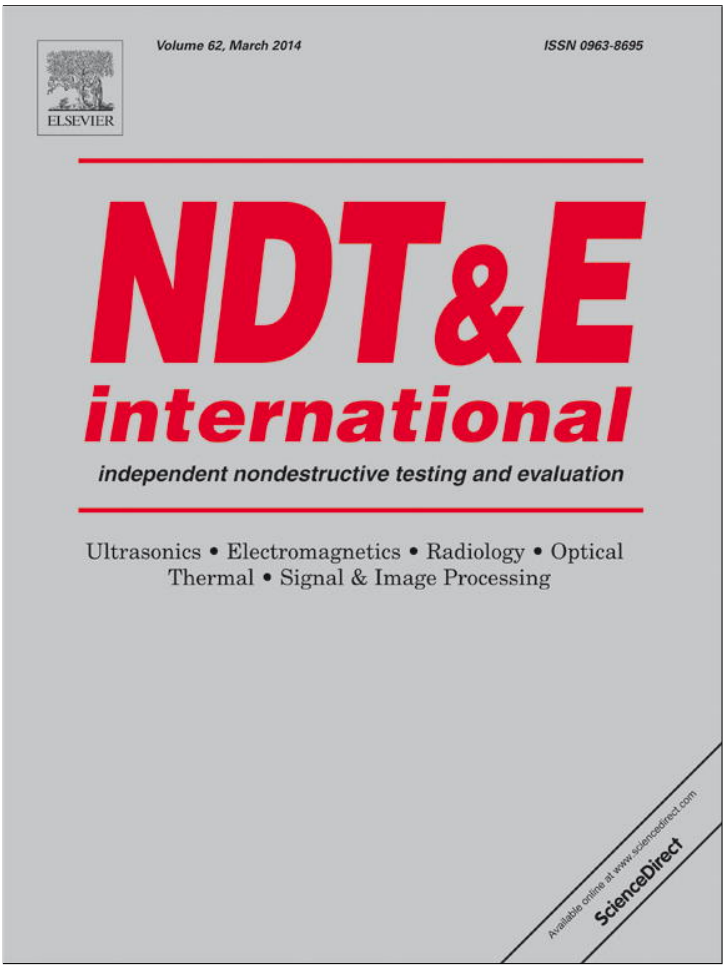

NDT&E International 62 (2014) 144–152

Contents lists available at ScienceDirect

NDT&E International

journal homepage: www.elsevier.com/locate/ndteint

Characterization of stress corrosion cracking in carbon steel using nonlinear Rayleigh surface waves

Daniel T. Zeitvogel [a], Kathryn H. Matlack [b,*], Jin-Yeon Kim [a], Laurence J. Jacobs [a,b], Preet M. Singh [c], Jianmin Qu [d]

[a] School of Civil and Environmental Engineering, Georgia Institute of Technology, Atlanta, GA 30332, USA
[b] Woodruff School of Mechanical Engineering, Georgia Institute of Technology, Atlanta, GA 30332, USA
[c] School of Materials Science and Engineering, Georgia Institute of Technology, Atlanta, GA 30332, USA
[d] Department of Civil and Environmental Engineering, Northwestern University, Evanston, IL 60208, USA

ARTICLE INFO

Article history:
Received 19 September 2013
Received in revised form
25 November 2013
Accepted 17 December 2013
Available online 27 December 2013

Keywords:
Nonlinear ultrasound
Nonlinear Rayleigh waves
Stress corrosion cracking

ABSTRACT

This research uses nonlinear Rayleigh surface waves to characterize stress corrosion cracking (SCC) damage in carbon steel. Cold rolled carbon steel is widely used for buried fuel pipelines; the environment surrounding these pipelines creates a mildly corrosive environment, which, in combination with an applied stress, can cause SCC. To ensure the safe operation of these structures, it is crucial that damage due to SCC be detected before their structural integrity is reduced by large cracks. In the early stages of SCC, microstructural changes such as dislocation formation and microcrack initiation occur, which have shown to considerably increase the acoustic nonlinearity of a material. These microstructural changes distort and generate higher harmonics in an initially monochromatic ultrasonic wave. This research considers four different levels of SCC induced in four separate 1018 steel specimens, a material which has a similar susceptibility to SCC as steel used for buried fuel pipelines. Then nonlinear ultrasonic measurements are performed before and after the SCC damage is induced. Nonlinear Rayleigh surface waves are utilized to detect the SCC damage that is concentrated near the material surface. The amplitudes of the fundamental and second harmonic waves are measured with contact wedge transducers at varying propagation distances to obtain the acoustic nonlinearity of the specimens as a function of SCC damage. The results show an increase in the measured acoustic nonlinearity in the early stages of SCC, indicating the feasibility of using this nonlinear ultrasonic method to detect the initiation of SCC in carbon steels.

1. Introduction

Stress corrosion cracking (SCC) of structural materials is a major concern across different industries, such as in pipelines for oil and fuel transport, and in nuclear reactor structural components. SCC is of specific concern in carbon steels, which are widely used for buried pipelines for gasoline transport. The surrounding ground water accumulated near the surface of these pipelines presents a mildly corrosive environment, which poses only a small risk of corrosion damage under normal circumstances. However, the combination of residual stresses at welded joints and pressure inside the pipe can raise the tensile stresses close to the yield strength of the material, which, under the influence of the corrosive environment, can lead to SCC [1–3]. Among the characteristics of SCC are crack initiation late in the lifetime of the structure and rapid crack growth and coalescence after crack initiation [3]. These characteristics necessitate a timely detection of the initiation of SCC damage prior to the formation of macrocracks. While macrocracks can be detected by linear ultrasonic techniques and/or by eddy current techniques [4], those nondestructive evaluation (NDE) methods are less suitable for the detection of microcracks and microstructural changes.

It has been shown that microstructural changes can be detected before the appearance of macroscopic damage by using nonlinear ultrasonic methods [5,6]. This is due to the fact that microstructural changes such as an increase in dislocation density distort ultrasonic waves, which leads to higher harmonics in an initially monochromatic wave. Since the energy of Rayleigh waves is concentrated near the surface, these waves are advantageous compared to bulk waves for the detection and characterization of SCC that initiates at the material surface. Additional advantages of Rayleigh waves include a longer propagation distance than for bulk waves, and required access to only one side of a specimen. Previous research has used nonlinear ultrasonic Rayleigh waves to detect fatigue damage in a nickel-base superalloy [7] and A36 steel [8] and thermal damage in 2205 duplex stainless steel [9]. In these studies, the acoustic nonlinearity was determined by measuring the normalized second harmonic amplitude at varying propagation distances. In contrast, Matlack et al. [10] changed the input frequency for a fixed receiver position (or propagation distance) to determine the acoustic nonlinearity.

* Corresponding author. Tel.: +1 4048942344.
E-mail address: katie.matlack@gmail.com (K.H. Matlack).

0963-8695/$ - see front matter © 2013 Elsevier Ltd. All rights reserved.
http://dx.doi.org/10.1016/j.ndteint.2013.12.005

This work investigates different levels of stress corrosion cracking in cold rolled AISI 1018 steel. While this material is not typically used for gasoline transport, the material's susceptibility to stress corrosion cracking is similar to steel used for gasoline transport such as carbon steel grade X65. Further, 1018 steel is much easier to obtain than, for example, carbon steel grade X65, in flat plate form in the length required for nonlinear ultrasonic Rayleigh wave measurements. Nonlinear Rayleigh surface waves are used to characterize SCC damage in this material by varying the wave propagation distance, following the techniques and procedures as described in previous work [7,8].

2. Theory

2.1. Nonlinear Rayleigh surface waves

Consider an isotropic, homogeneous, nonlinear elastic half space in which Rayleigh waves are propagating along its free surface. As the fundamental wave propagates, a second harmonic wave is generated due to the nonlinearity of the material. For a plane Rayleigh wave, a critical relationship is [7]

$$\frac{A_2}{A_1^2} \propto \frac{\omega^2 x \beta}{c_R^2} \tag{1}$$

where A_1 and A_2 are, respectively, the amplitudes of the fundamental and second harmonic waves, ω is the fundamental angular frequency, x is the propagation distance, β is the acoustic nonlinearity parameter, and c_R is the Rayleigh wave speed. Since the wave speed is constant and the excitation frequency is kept constant, a relative measure of β can be obtained by measuring the fundamental and second harmonic amplitudes at varying propagation distances. In this case, the nonlinearity parameter can be expressed as

$$\beta = \frac{A_2}{x A_1^2 C} \tag{2}$$

where C contains all constant parameters. Note that Eq. (2) is not an exact expression when the fundamental wave is generated by a finite-sized transducer, and both the fundamental and second harmonic waves are received by finite-sized transducers. However, the linear relationship between A_2/A_1^2 as a function of propagation distance, x in Eq. (1) has been shown both theoretically and experimentally to be a good approximation for a short propagation distance in the far field [11]. In the current experiments, A_2/A_1^2 is measured over x, such that the slope is $\beta' = \beta/C$, where β' is a calibrated acoustic nonlinearity parameter that is proportional to the absolute acoustic nonlinearity parameter, β.

2.2. Stress corrosion cracking

SCC can occur under certain environmental conditions, specifically the combination of a mildly corrosive environment and tensile stresses. SCC often occurs in environmental conditions that are generally considered harmless and can affect materials that are corroded uniformly at a very low corrosion rate. Even stainless steel that is exposed to drinking water can be affected by SCC, due to the amount of chloride in drinking water when certain conditions are met [12].

The process of SCC in carbon steels starts with the formation of an iron oxide layer on the surface. This film normally protects the underlying material from being exposed to the corrosive environment. However, when a sufficiently high tensile stress is applied, the film ruptures in areas of localized plasticity, exposing the bare metal surface to the corrosive environment. Anodic dissolution at the exposed surface leads to crack initiation and propagation [1], and high stresses near crack tips induce generation of dislocations which will subsequently move around and pile up.

While these microstructural changes have little influence on the material's overall mechanical properties, they lead to an increase of the acoustic nonlinearity. As shown by Cantrell [13], the acoustic nonlinearity increases with an increased dislocation density. Furthermore, the acoustic nonlinearity is increased significantly by the formation of microcracks that cause contact nonlinearity. With increased initiation and propagation of the microcracks, they coalesce to form macrocracks. These macrocracks are expected to cause an increase in attenuation at the higher frequencies of the second (and higher) harmonic waves, which leads to a significant drop in the apparent measured acoustic nonlinearity parameter. This effect has been shown at later stages of fatigue life, for example, in [14,7], however, these later stages of SCC damage are beyond the scope of this work.

3. Specimens and damage

The specimens under investigation are machined from cold rolled 1018 carbon steel. The steel was annealed to ensure a lamellar pearlite microstructure, and cold drawn; the chemical composition is given in Table 1. An undamaged sample was sectioned, polished, and etched in 2% Nital to visualize the pearlite microstructure, which can be seen in Fig. 1. Here, the darker regions seen in both optical micrographs ((a) 200× and (b) 500× magnification) show the pearlite microstructure, and the image at higher magnification shows the alternating layers of cementite and ferrite regions. The material has a nominal yield strength of 372 MPa (54,000 psi) and tensile strength of 441 MPa (64,000 psi). The geometry of the specimens is a dog-bone shape typical of tensile test specimens. In order to provide a suitable geometry for Rayleigh wave propagation and ultrasonic measurements, the specimens have a long test section of 254 mm. Three specimens (Specimens #2–4) have a width of 18.5 mm and a thickness of 5.1 mm, while due to machining issues Specimen 1 has a width of 18.5 mm and a thickness of 3.8 mm. The surface of the test section is carefully sanded and polished with up to 2000 grit polish paper to minimize premature SCC initiation at sites of local stress concentrations, as well as to minimize the influence of surface roughness on the propagating Rayleigh surface waves.

SCC damage is induced in the specimens using a stress corrosion cell where the specimen is loaded and exposed to a corrosive environment which has shown to produce SCC [3,15,10]. These experimental parameters are representative of the environment and loading conditions in buried pipelines. The corrosion cell consists of a glass tube which is closed and sealed on both ends. The lids are designed to accommodate insertion of a reference platinum electrode to control the applied potential, and a thermocouple with which to control the temperature of the aqueous solution. An illustration of such a setup is shown in Fig. 2. The specimens are immersed in an aqueous solution of 1N sodium carbonate (Na_2CO_3) and 1N sodium bicarbonate ($NaHCO_3$). This solution is kept at a temperature of 70 °C using heat tape wrapped around the corrosion cell, while an electrochemical potential of −650 mV vs. Saturated Calomel Electrode (SCE) is applied using a potentiostat. The specimen is then simultaneously subjected to a static tensile stress over a period of five days in this corrosive environment. The level of applied tensile stress varies among the

Table 1
Chemical composition (wt%) for cold rolled 1018 carbon steel specimens.

C	Mn	Si	S	P	Fe
0.16	0.78	0.26	0.021	0.005	As remainder

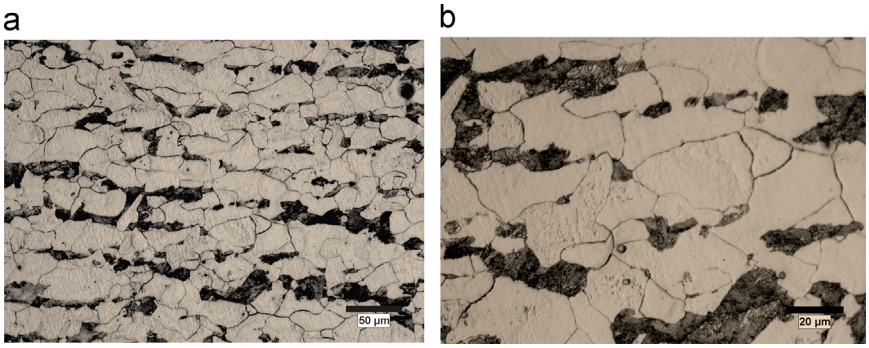

Fig. 1. Optical micrographs of 1018 steel microstructure at (a) 200× magnification and (b) 500× magnification.

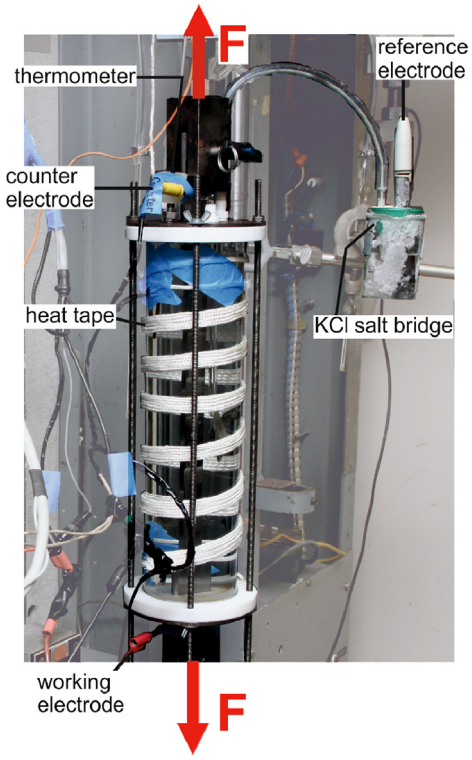

Fig. 2. Setup of stress corrosion cell.

four individual specimens to create different levels of SCC damage. Further details on this constant stress experimental method can be found in [16].

In order to assess the extent of the SCC damage, the corroded specimens are examined using an optical microscope. The surface, which is covered by a thin iron oxide layer, is carefully removed by hand polishing in order to get an unobstructed view of the metal beneath the iron oxide. It is important to remove only the iron oxide layer and not the underlying damaged material or cracks, and note that any scratches obtained during the polish process were much smaller than the Rayleigh wavelength and will not influence the attenuation or nonlinearity of the propagating Rayleigh waves. For a quantitative evaluation of the amount of SCC damage, ten adjoining micrographs at 500x magnification are taken out of a representative area in the middle of the damaged section of each specimen. In these micrographs, the number and length of visible cracks are counted and measured. Since stress corrosion cracks can only initiate on the surface of the material, the number of cracks per unit area on the surface is equivalent to the number of cracks per volume. This is not, however, equivalent to a "damage volume" of cracks. Crack depth has been shown

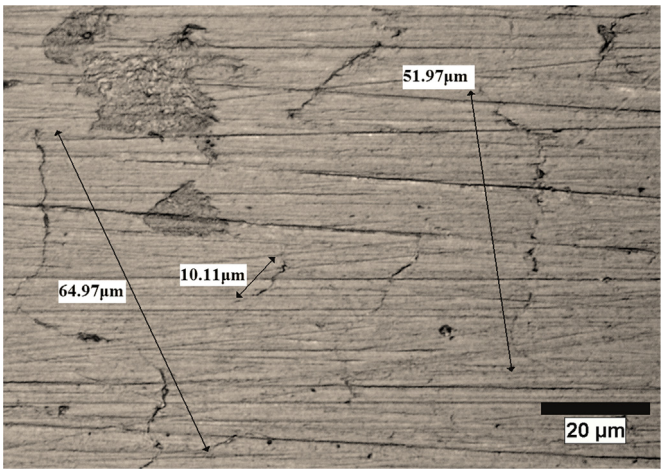

Fig. 3. Optical micrograph of various cracks in Specimen 4 showing highest level of SCC damage, at 500× magnification.

previously to be related to the crack length as $0.1 < d/(l/2) < 0.2$ [15]. So, while not directly observable, the total crack surface area, S, can be estimated by $S = AN$, where $A = \pi(l/2)d/2$ is the area of a closed elliptical-shaped surface crack.

A representative optical micrograph at 500× magnification with visible stress corrosion cracks of a variety of sizes is shown in Fig. 3. Not all visible cracks are indicated on the image in Fig. 3 to ensure clarity. Note that the specific pearlitic microstructure of the material will not affect SCC propagation in this case. SCC of carbon steel in carbonate–bicarbonate environments has been shown previously to be intergranular, so the specific microstructure within grains will not affect SCC. A cross section of Specimen 4 was also mounted such that crack depth could be visualized. Two separate optical micrographs showing different cracks are shown in Fig. 4, both at 500× magnification. It should be pointed out that it is difficult to measure the true crack depth, since one cannot ensure the cross section cut would catch the maximum depth of the elliptically-shaped crack. The micrographs presented in both Figs. 3 and 4 provide evidence that stress corrosion cracks have formed.

4. Nonlinear ultrasonic measurements

Rayleigh waves are generated and detected using contact wedge transducers. A commercial piezoelectric longitudinal wave transducer with a center frequency of 2.25 MHz and a diameter of 12.7 mm is fixed to an acrylic wedge with an angle of 67°, which is clamped to the specimen. At this Rayleigh critical angle, the longitudinal wave emitted by the transducer is converted to a Rayleigh surface wave in the specimen. A transducer with a center

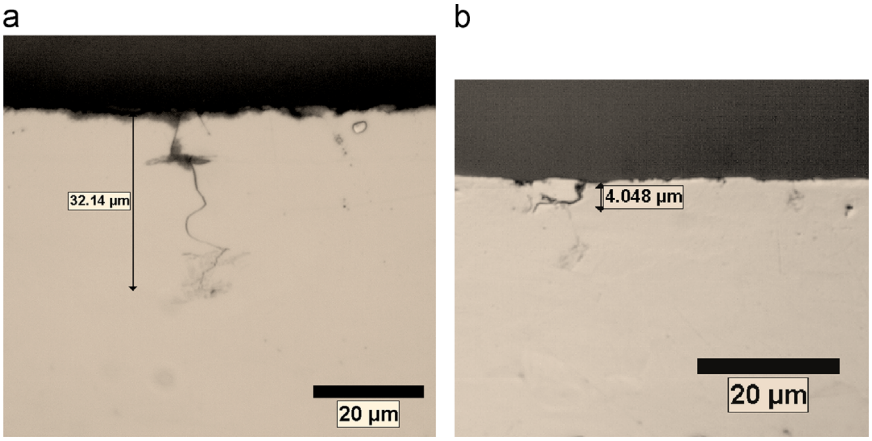

Fig. 4. Optical micrographs of two separate crack depths, taken at 500 × magnification.

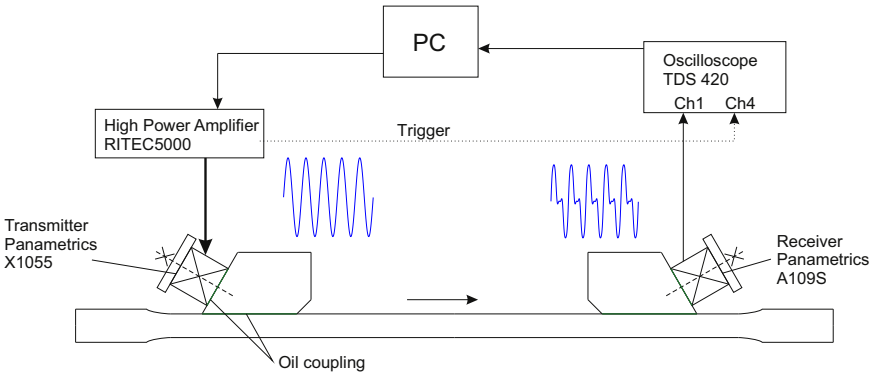

Fig. 5. Setup for nonlinear ultrasonic measurements.

frequency of 5 MHz is attached to a wedge with the same angle to detect the transmitted Rayleigh waves at varying propagation distances. A 2.25 MHz tone burst that is generated by a high-power gated amplifier (RITEC RAM-5000) is fed into the transmitting transducer. The received signals are recorded with an oscilloscope (Tektronix TDS 420) and 507 signal samples are averaged to improve signal-to-noise ratio (SNR). The nonlinear ultrasonic measurement setup is illustrated in Fig. 5.

In order to obtain the acoustic nonlinearity parameter, β, measurements are taken at varying propagation distances. Note that it is also possible to calculate the acoustic nonlinearity parameter by varying the fundamental frequency [10]. While this method eliminates the coupling contact variability since the wedges remain at the same locations on the specimen, it also introduces other effects such as the frequency response of the transducers and potential frequency-dependent nonlinearities of the electronic instrumentation, which are difficult to compensate for.

The measurement technique of varying propagation distances used in this work eliminates the influence of these frequency-dependent nonlinearities, but the potential for large variations in the coupling contact condition between the wedges and the specimen surface for different measurements need to be carefully handled. To obtain statistically acceptable data, five sets of measurements are taken for each specimen. Each set of measurements consists of 19 individual measurements at propagation distances that vary from 50 mm to 140 mm in increments of 5 mm. In order to make the measurements comparable, the position of the transmitter is placed in the same location on each specimen for all measurements taken before and after SCC damage.

At the first few shorter propagation distances, the second harmonic wave has not yet appreciably grown (the near field of the second harmonic), while at the farthest propagation distances, the nonlinearity parameter no longer increases due to the attenuation (caused by absorption, diffraction, and scattering), such that there is a limited range of propagation distances for which Eq. (1) is valid. At the propagation distances in between these two zones, the normalized second harmonic amplitude A_2/A_1^2 increases in an approximately linear fashion. The approximate near field to far field distance of the transducer can be calculated using the relation $x_N = a^2/\lambda_R$, where a is the radius of the transducer (ignoring the beam spreading in the wedge) and λ_R is the wavelength of the Rayleigh wave. The Rayleigh wave velocity was measured to be 2989 m/s in the 1018 steel, such that the wavelengths of the propagating first and second harmonic Rayleigh waves were 1.3 mm and 0.66 mm, respectively. This gives a distance x_N of 30 mm for the fundamental wave and x_N of 60 mm for the second harmonic wave. The usable range of propagation distances in the measurement starts at about 60 mm and ends at about 120 mm. However, these boundaries vary slightly for different specimens so that the starting and ending positions have to be selected manually (in post-processing) for each specimen, particularly since attenuation of the higher frequencies is expected to increase with increasing SCC damage. As shown in Eq. (2) the slope of the best fit line, β', of the normalized second harmonic amplitude versus the propagation distance is directly proportional to the acoustic nonlinearity parameter, β.

It should be noted that some geometrical effects on the Rayleigh wave propagation are expected. The width of the specimens (18.5 mm) is expected to affect the diffraction pattern of the Rayleigh waves in these experiments, compared to a diffraction pattern in an infinitely wide medium. Typically, the energy of the Rayleigh wave beam would spread in the width direction as the

wave propagates, but with the current geometry, the edges would prevent this energy spread. Further, any small misalignment of the transmitting wedge that would hinder the waves from propagating perfectly parallel to the sides would cause reflections from the sides. In terms of the specimen thickness effects, it is known that the displacement and stress of the propagating Rayleigh wave is negligible after about 1.5λ. Given the longest wavelength considered in these experiments (1.3 mm), the displacement of the Rayleigh wave is negligible beyond a depth of 2 mm. So, the specimens with a thickness of 5.1 mm should be thick enough to ensure Rayleigh wave propagation. However, since specimen 1 was slightly thinner at 3.8 mm and since waves are excited at a small range of angles with wedge excitation, it is expected there will be some longitudinal wave components that propagate through to the specimen that will reflect off the bottom surface. Since longitudinal waves propagate at almost twice the wavespeed as the Rayleigh waves, it is possible components from these waves influenced the measured amplitudes of the Rayleigh waves. While these effects will influence the propagating first and second harmonic waves, results show that the diffraction of the A_1 wave does not change after SCC damage, so comparing results of a single specimen before and after damage should eliminate specimen geometrical effects to measured wave amplitudes.

5. Results

5.1. Nonlinear Rayleigh wave results

As mentioned in Section 3, all parameters except the applied tensile stress are kept constant during the corrosion process. In order to accelerate the SCC process, the applied tensile stress ranges from the nominal yield stress to 10% over the nominal yield stress and held in the same corrosive environment. It is important to note that during the corrosion process of Specimen #3, the potentiostat failed to maintain a constant potential. As a result, only very small cracks can be observed under the microscope and there is no significant change in the measured acoustic nonlinearity parameter for this specimen.

Fig. 6 shows the measured nonlinearity of Specimen 1 in both the undamaged and damaged conditions, in terms of measured A_2/A_1^2 over propagation distance, and increase in β'. Specimen 1 is loaded at the nominal yield stress. To illustrate the near field effect

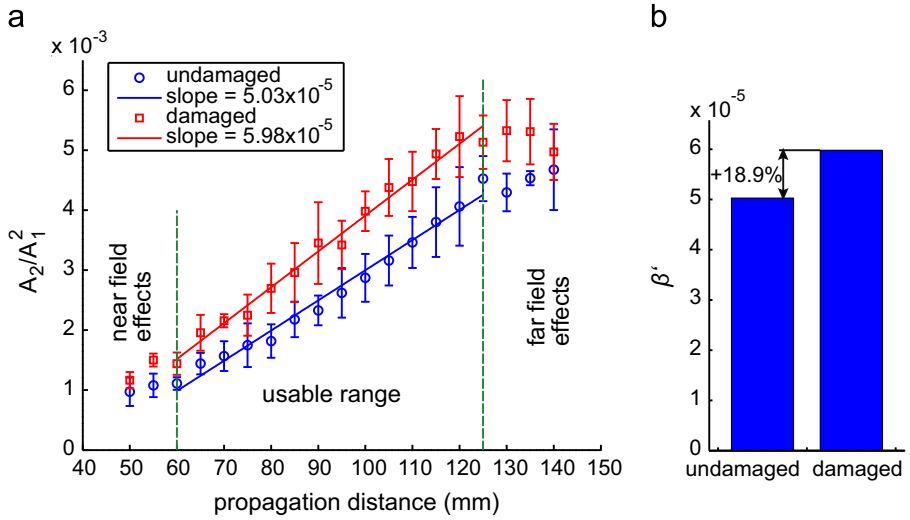

Fig. 6. Comparison of nonlinearity of undamaged and damaged specimen #1 loaded at nominal yield stress, in terms of (a) measured $A_2/A_1{}^2$ over propagation distance, and (b) β'.

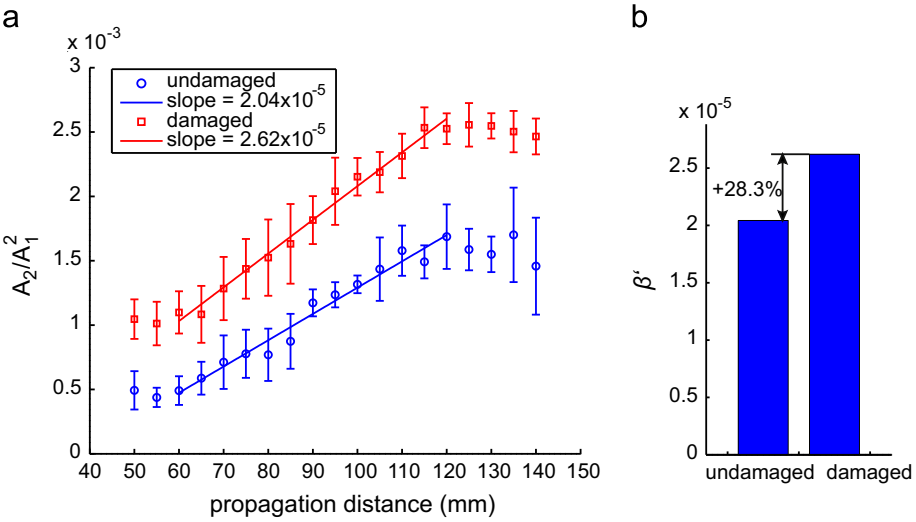

Fig. 7. Comparison of nonlinearity of undamaged and damaged Specimen #2 loaded at 7.8% over nominal yield stress, in terms of (a) measured $A_2/A_1{}^2$ over propagation distance, and (b) β'.

and the attenuation effect as discussed in Section 4, Fig. 6 has these regions clearly marked. The slope of the best fit line of the damaged specimen is 18.9% higher than that of the undamaged specimen, which indicates a noticeable increase in nonlinearity.

Likewise, Figs. 7–9 show the measured nonlinearity of Specimens 2, 3, and 4 in terms of measured A_2/A_1^2 over propagation distance and increase in β'. Note that Specimen 2 is loaded at 7.8% above the nominal yield stress, and Specimens 3 and 4 are loaded at 10% above the nominal yield stress. The results of Specimens 1, 2, and 4 show considerable increases in the measured nonlinearity, whereas the change in the measured nonlinearity of Specimen 3 is quite small. Note that variations in microstructure due to processing and machining will cause differences in the baseline β' of specimens in their undamaged state. This is why the measured acoustic nonlinearity parameter of the specimens due to SCC damage is always compared to the measured nonlinearity parameter of the undamaged specimen.

5.2. Linear Rayleigh wave results

The trends of the measured first harmonic amplitude over propagation distance before and after SCC damage are shown in Fig. 10(a) Specimen 1, and (b) Specimen 4. Specimens 1 and 4 represent the least and most amount of induced SCC damage, respectively. As in previous plots, data points here represent an average over five separate measurements, and error bars represent one standard deviation from the mean. While a direct measure of the attenuation coefficient was not made, these results show no detectable change in the propagating first harmonic wave when compared to the variation in the measurements. Therefore, it can be concluded that the attenuation coefficient of the first harmonic wave does not significantly change due to the SCC damage. The difference in the diffraction trend of Specimen 1 compared to Specimen 4 is likely due to differences in attenuation of the orginal specimen, and the smaller cross section. Further, since crack depth is in the order of 1% of the wavelength of A_2 (0.66 mm) and an even smaller percentage of the wavelength of A_1, it is expected that the attenuation change due to cracks is quite small, since cracks are thus in the weak scattering regime of the wavelengths of the propagating waves. So, it can be concluded that the condition that $\beta \propto A_2/A_1^2$ as described in Eq. (1) is met and the increase in the parameter β' is due to nonlinear effects.

The velocity of each specimen and damage level is given in Table 2 below. The velocity was calculated simultaneously with the nonlinear measurements, by correlating the received time signals from different propagation distances to extract the difference in arrival times. The velocities reported represent an average over the longer propagation distances (90 mm to 140 mm) over all five

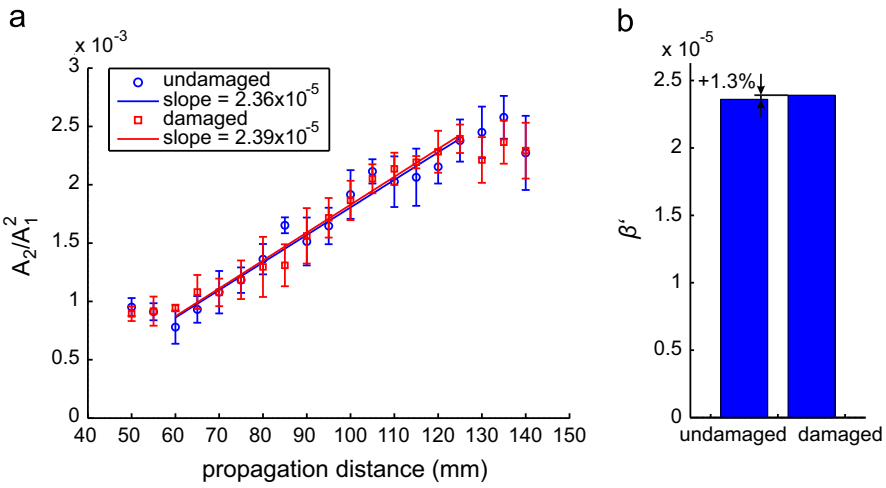

Fig. 8. Comparison of nonlinearity of undamaged and damaged Specimen #3 loaded at 10% over nominal yield stress, in terms of (a) measured $A_2/A_1{}^2$ over propagation distance, and (b) β'.

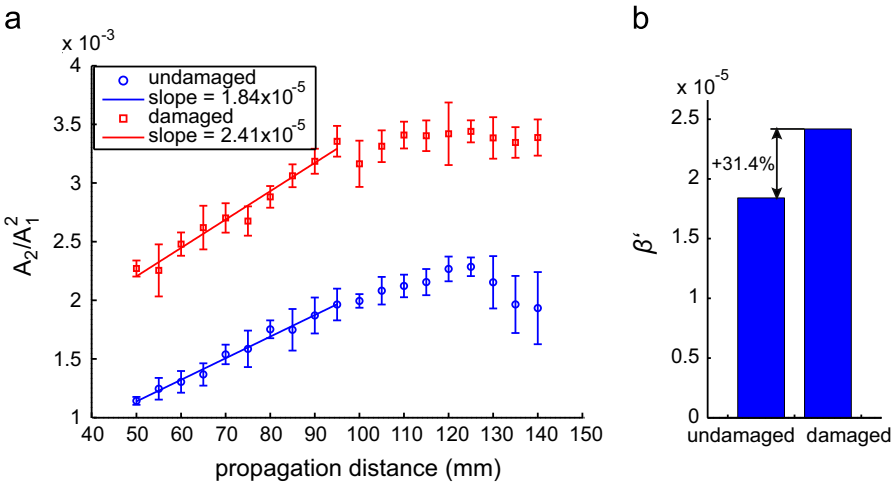

Fig. 9. Comparison of nonlinearity of undamaged and damaged Specimen #4 loaded at 10% over nominal yield stress, in terms of (a) measured $A_2/A_1{}^2$ over propagation distance, and (b) β'.

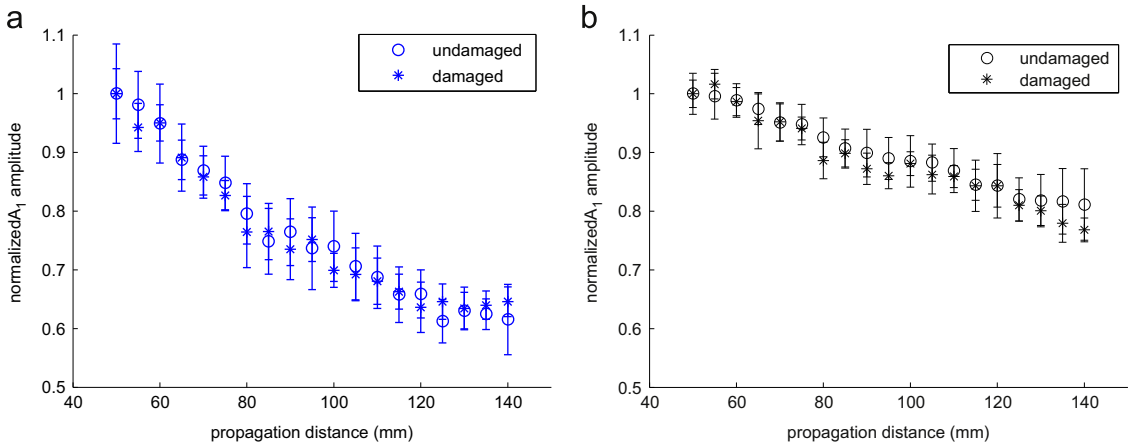

Fig. 10. Trend of measured first harmonic amplitude over propagation distance before and after SCC damage for (a) Specimen #1 and (b) Specimen #4.

Table 2
Average measured Rayleigh wave velocity, for each specimen in the undamaged and SCC damaged case.

Specimen #	Undamaged velocity (m/s)	Damaged velocity (m/s)
1	2989.0 ± 8.1	2979.6 ± 23.7
2	3000.2 ± 21.4	2987.5 ± 18.3
3	2997.3 ± 8.6	2998.9 ± 11.6
4	2984.5 ± 19.5	2975.6 ± 8.2

Table 3
Normalized applied stress and results of Specimens 1, 2, and 4.

Specimen #	Normalized applied stress	β/β_0
1	1.00	1.189
2	1.078	1.283
4	1.10	1.314

measurements. Results show that the wave was propagating with a velocity typical of Rayleigh waves in steel, which is further evidence that the waves were in fact propagating as Rayleigh waves despite the confined cross section of the specimen geometries. Furthermore, results show less than a 1% change from the undamaged state to damaged SCC state, showing that wave velocity measurements are not sensitive to SCC damage of the magnitude investigated in this work.

5.3. Comparison of the nonlinear ultrasonic results

The results from the nonlinear ultrasonic measurements of Specimens 1, 2, and 4 are compared in terms of the applied stress normalized by the nominal yield stress. The percentage change in the acoustic nonlinearity parameter for each specimen that is normalized with that of the undamaged specimen is plotted versus the normalized applied stress level. These results are summarized in Table 3 and shown in Fig. 11.

Fig. 11 shows a tendency toward a linear relationship between the applied stress and the increase in the measured nonlinearity parameter by as much as 30%. This result, however, does not include the anomalous behavior of Specimen 3. Assume that both the number density and average size of cracks are the indicators for the amount of damage accumulated in the material. In Fig. 12, the percent change in the nonlinearity parameter is plotted against the crack number density ($1/\text{mm}^3$), determined as described in Section 3. Fig. 13 compares the percent change in the nonlinearity parameter to the average crack length. Note that

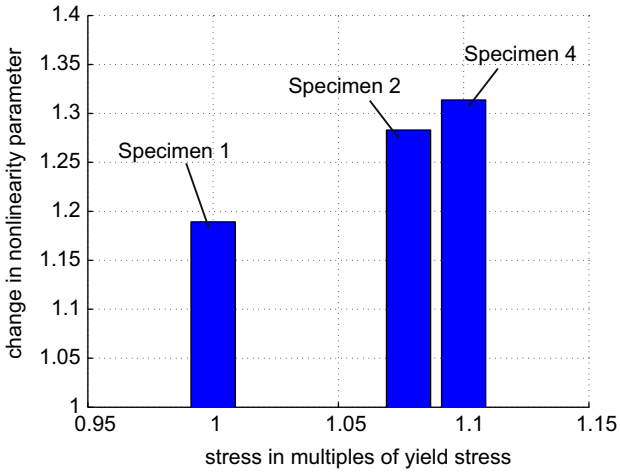

Fig. 11. Change in β' compared to applied stress.

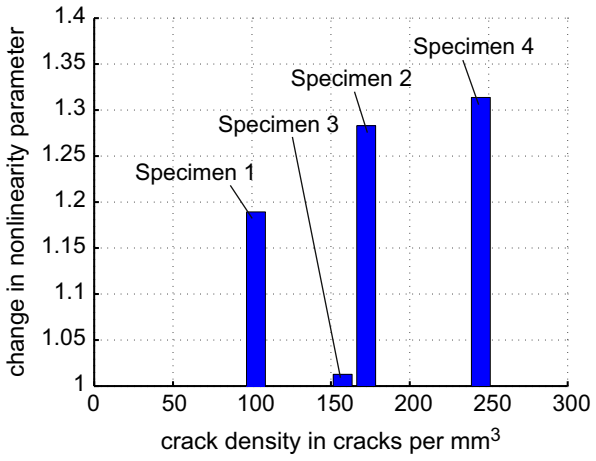

Fig. 12. Change in β' compared to crack number density.

since β' is expected to be a function of both crack length and crack density, i.e., $\beta' = f(L, N)$, and since Fig. 12 shows the trend in β' over different crack densities but *not* constant crack lengths (and vice versa for Fig. 13), the dependency of β' on these individual parameters cannot be extracted from these plots alone.

These comparisons show, with the exception of Specimen 3 (with its failed potentiostat) in Fig. 12, a general tendency of increasing nonlinearity parameter with both the crack length and

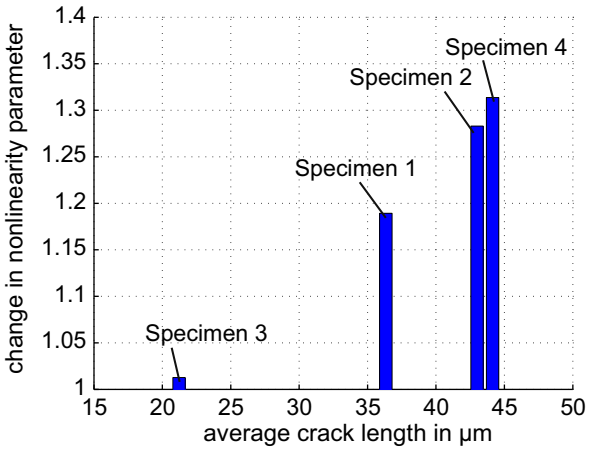

Fig. 13. Change in β' compared to average crack length.

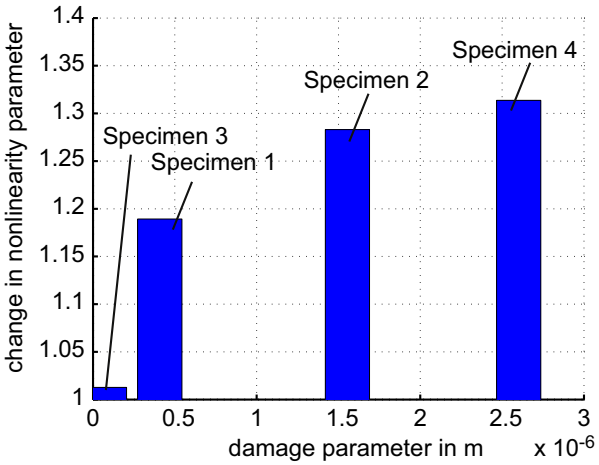

Fig. 14. Change in β' compared to the damage parameter p_{dmg}.

Table 4
Damage parameter of specimens.

Specimen #	$\langle l^4 \rangle$ (10^{-18} m^4)	Average crack number density N (1/mm^3)	Damage parameter p_{dmg} (10^{-6} m)
1	3.98	102.54	0.408
2	9.02	172.38	1.555
3	0.44	157.48	0.0698
4	10.62	245.02	2.601

the crack number density. This implies that both the crack number density and the crack size (or length) increase with the progress of SCC in this material. This also suggests the introduction of a damage parameter, which can take into account both the effects of the crack size and number density that reflects the amount of the SCC damage. Nazarov and Sutin [17] proposed a model for the nonlinearity of a solid with randomly oriented, randomly distributed, closed cracks. The mechanism of the elastic nonlinearity is the Hertzian contact of two rough surfaces of a closed crack, with the gap between the two surfaces being disturbed by ultrasonic waves. Their model suggests that the nonlinearity parameter depends on the fourth power of the crack depth, and is directly proportional to the crack number density. As mentioned in Section 3, the crack depth cannot be directly measured. However, due to the approximately linear relationship between the crack depth and length, and assuming an elliptical crack, the crack length is used for this examination.

While the cracks in the present experiment are aligned perpendicular to the loading direction (and also perpendicular to the direction of wave propagation) and the crack lengths have some statistical distribution, it is assumed that the same dependence holds as in a solid with random crack size and orientation. The cracks in the specimens in this study were observed to be closed after removal of the applied tensile load. Therefore, based on [17], a possible damage parameter is defined as

$$p_{dmg} = N\langle l^4 \rangle, \tag{3}$$

where N is the average crack number density and $\langle l^4 \rangle$ is the average of the fourth power of crack length. The respective damage parameters of the individual specimens are listed in Table 4 and depicted in Fig. 14.

For all specimens examined in this study, a larger damage parameter results in a higher change in acoustic nonlinearity, and, excluding Specimen 3, the acoustic nonlinearity appears to be proportional to the damage parameter, as evident in Fig. 14. This trend indicates that the acoustic nonlinearity parameter is proportional to the fourth power of crack length for the damage levels of Specimens 1, 2, and 4, however, to affirm such a relationship, more data points (measured acoustic nonlinearity on more specimens with different damage parameters) are needed. So, while it is clear the acoustic nonlinearity parameter is sensitive to the crack length, more investigations are needed in order to fully interpret Figs. 12–14, in terms of the relation between the acoustic nonlinearity parameter and the damage parameter and microcrack properties. This sensitivity to crack length has important implications for detecting SCC damage – prior to macroscopic cracking, it is known that SCC is characterized by rapid crack growth and coalescence after microcrack initiation [3].

Specimen 3, which has a small, but non negligible amount of damage, shows only a small increase in acoustic nonlinearity, which falls within the standard deviation of the measurements. If the acoustic nonlinearity parameter is proportional to the fourth power of the crack length as defined in the damage parameter, the crack length contributes much more significantly than the crack number density to which the nonlinearity parameter is proportional. This is evident in the comparison of Figs. 12 and 13, and in the much smaller average crack length in Specimen 3 compared to the other specimens, as reported in Table 4. It should also be noted that the dislocations produced during the SCC process contribute to the measured nonlinearity in this investigation. While the microcracks produce much stronger nonlinearity than dislocations [18], micromechanical modeling and analysis is needed for a more quantitative interpretation of the results in Figs. 11–14.

6. Conclusion

This research presents a nonlinear ultrasonic method to characterize damage due to stress corrosion cracking (SCC) in 1018 carbon steel by measuring changes in the acoustic nonlinearity of Rayleigh surface waves. Damage is induced in four specimens by applying high amounts of tensile stress while the specimens are immersed in a SCC causing environment. Rayleigh waves are generated and detected using wedge transducers to measure the normalized second harmonic amplitude. This normalized amplitude A_2/A_1^2 shows an approximately linear relationship over propagation distance, where the slope of the linear fit is proportional to the acoustic nonlinearity parameter, β. The percent increase in the measured acoustic nonlinearity parameter due to SCC damage is compared to the damage quantified under an optical microscope – that is, the length and number density of visible microcracks. A damage parameter is then

defined by assuming that the underlying mechanism of the observed nonlinearity is the Hertzian contact of closed cracks. This parameter is used to interpret the change in measured acoustic nonlinearity due to SCC. For a certain range of SCC damage, the change in acoustic nonlinearity parameter shows a linear correlation with the defined damaged parameter. This analysis shows that the acoustic nonlinearity parameter strongly depends on the crack length of the microcracks.

Acknowledgments

The authors would like to thank the Deutscher Akademischer Austauschdienst (DAAD) for providing partial financial support. The help of Jamshad Mahmood with the SCC experiments is greatly appreciated.

References

[1] Jones RH, Ricker RE. Mechanisms of stress-corrosion cracking. In: Jones RH, editor. Stress-corrosion cracking. Materials Park, Ohio: ASM International; 1992 (p. 1–40).
[2] Asher SL, Singh PM. Role of stress in transgranular stress corrosion cracking of transmission pipelines in near-neutral pH environments. Corrosion 2009;65 (2):79–87.
[3] Parkins RN, Singh PM. Stress corrosion crack coalescence. Corrosion 1990;46 (6):485–99.
[4] Chen Z, Janousek L, Yusa N, Miya K. A nondestructive strategy for the distinction of natural fatigue and stress corrosion cracks based on signals from eddy current testing. J Press Vessel Technol, Trans ASME 2007;129:719–28.
[5] Kim J-Y, Jacobs LJ, Qu J, Littles JW. Experimental characterization of fatigue damage in a nickel-base superalloy using nonlinear ultrasonic waves. J Acoust Soc Am 2006;120(3):1266–73.
[6] Liu M, Kim J-Y, Jacobs L, Qu J. Experimental study of nonlinear Rayleigh wave propagation in shot-peened aluminum plates – feasibility of measuring residual stress. NDT&E Int 2011;44:67–74.
[7] Herrmann J, Kim J-Y, Jacobs LJ, Qu J, Littles JW, Savage MF. Assessment of material damage in a nickel-base superalloy using nonlinear Rayleigh surface waves. J. Appl. Phys. 2006;99(12):124913-1.
[8] Walker SV, Kim J-Y, Qu J, Jacobs LJ. Fatigue damage evaluation in A36 steel using nonlinear Rayleigh surface waves. NDT&E Int 2012;48:10–5.
[9] Ruiz A, Ortiz N, Medina A, Kim J-Y, Jacobs LJ. Application of ultrasonic methods for early detection of thermal damage in 2205 duplex stainless steel. NDT&E Int 2013;54:19–26.
[10] Matlack KH, Kim J-Y, Jacobs LJ, Qu J, Singh PM. Nonlinear Rayleigh waves to detect initial damage leading to stress corrosion cracking in carbon steel. In: Thompson DO, Chimenti DE, editors. Review of progress in quantitative nondestructive evaluation, 31B. Burlington, VT: American Institute of Physics; 2011 (p. 1452–1459).
[11] Huang C.-L.. Effect of beam diffraction on nonlinear Rayleigh surface wave measurements [Masters thesis]. Georgia Institute of Technology; 2013.
[12] Staehle RW. Comments on the history, engineering and science of stress corrosion cracking. In: Staehle RW, Forty AJ, Rooyen Dv, editors. Proceedings of conference fundamental aspects of stress corrosion cracking, Houston, Texas. National Association of Corrosion Engineers; 1967, p. 3–14.
[13] Cantrell JH. Substructural organization, dislocation plasticity and harmonic generation in cyclically stressed wavy slip metals. Proc R Soc Lond, Ser A (Math, Phys and Eng Sci) 2004;460(2043):757–80.
[14] Barnard DJ, Brasche LJH, Raulerson D, Degtyar AD. Monitoring fatigue damage accumulation with Rayleigh wave harmonic generation measurements. In: Thompson DO, Chimenti DE, editors. Review of progress in quantitative nondestructive evaluation, 22. AIP; 2003 (p. 1393–1400).
[15] Singh PM. Stress corrosion cracking of carbon steel and inconel 600 [Ph.D. thesis], University of Newcastle upon Tyne; 1989.
[16] Goodman L, Singh PM, Mahmood J, Braswell M, Raji S. Formation and breakdown of passive films on x65 pipeline steel in fuel grade ethanol environments and its implications for stress corrosion cracking. In: Proceedings of NACE international, Salt Lake City, UT. Paper # C2012-0001481, CORROSION-2012; 2012.
[17] Nazarov VE, Sutin AM. Nonlinear elastic constants of solids with cracks. J Acoust Soc Am 1997;102(6):3349–54.
[18] Cantrell JH. Quantitative assessment of fatigue damage accumulation in wavy slip metals from acoustic harmonic generation. Philos Mag 2006;86(11): 1539–54.